SCIENTIFIC CMOS SENSORS IN ASTRONOMY: QHY600 AND QHY411

Miguel R. Alarcon*(1), Javier Licandro(1), Miquel Serra-Ricart(1), Enrique Joven(1), and Vicens Gaitan(2)

(1)*Instituto de Astrofísica de Canarias (IAC), C/ Vía Láctea s/n, E-38205 La Laguna, Canarias, Spain. *Email: mra@iac.es*

(2)*Aplicaciones en Informática Avanzada (AIA), E-08172 Sant Cugat del Vallès, Catalonia, Spain*

ABSTRACT

Scientific CMOS is developing quickly in recent years, due to its low cost, replicability, and advantages over CCD such as high frame rate, low readout noise or near-zero readout time. With the development of the first back-illuminated models, these sensors are starting to be used in Astronomy, so it is worth studying their characteristics, their advantages and weaknesses to be considered. In this work, we present the results of the laboratory characterisation of the IMX455 and IMX411 sensors, integrated into the QHY600 and QHY411 cameras respectively. These are large (36x24 and 54x40 mm) native 16-bit sensors with 3.76 micron pixels sensitive in the optical range. Their quantum efficiency has been found to peak at 80% at 475 nm, with 40% at 700 nm and 10% at 900 nm. Their linearity and photon transfer performance has been evaluated, as well as their dark behaviour. They showed a low dark current, but also a presence of warm pixels of about a 0.024% in the QHY600 and 0.005% in the QHY411. The effect of random telegraph noise, also called *Salt&Pepper* noise, has been also analysed, being one of the most relevant issues to be addressed with these two sensors. Some sky tests are also presented to discuss the their astronomical performance and future possibilities.

Keywords: Astronomical sensors; Imaging instruments; CMOS.

1. INTRODUCTION

Over the last two decades, the rise of certain alternative technologies has undermined the prevalence of CCD sensors. The development of Complementary Metal-Oxide-Semiconductor (CMOS) image sensors started to emerge in the 1990s [4], but they still had disadvantages over CCDs, such as lower dynamic range (DR) and poorer linearity and sensitivity [2]. CMOS soon established itself in the consumer market, but its inherent constraints restricted its application in certain fields, especially those related to science.

To overcome the typical limitations of CMOS, so-called scientific CMOS (sCMOS) were developed, first introduced in 2009 as a result of collaboration between Andor Technology, Fairchild Imaging (BAE Systems) and PCO Imaging [3]. This new generation of sensors combined high frame rates, reasonable pixel and sensor sizes, quantum efficiencies comparable to CCDs–especially back-illuminated (BI) sCMOS [8]– and a considerable reduction in the noise levels traditionally associated with CMOS.

Many leading manufacturers are now developing instrumentation based on next-generation sCMOS sensors, but their suitability for general use in Astronomy is still largely unexplored. One of the most widespread sensors are those from the Sony IMX series, which are being included in large projects such as the Argus Optical Array [5] or ATLAS-Teide (Licandro et al., *New telescopes and radars* session) because of their low cost and capability for wide-field and high-cadence surveys. In this work, we present the results of the laboratory characterization of the sCMOS BI Sony IMX455M and IMX411M sensors, integrated into the QHY600M and QHY411M cameras.

2. METHODS

The QHY600M[1] camera is based on the back-illuminated IMX455 monochrome sensor manufactured by SONY, a full-frame (35 mm format) sensor with 9576×6388, 3.76 μm square pixels. The QHY411M[2] camera is based on the same manufacturer IMX411 monochrome sensor, also back-illuminated but a larger sensor size, with 14304×10748 (equivalent to medium-format cameras, 54×40 mm). They are native ADC sampled at 16-bit, which is a significant change from previous generations of sCMOS sensors based on 12–bit image merging [6]. Both sensors, especially the IMX455, are also used in cameras from other manufactures, e.g. Atik Apx60, ZWO ASI6200MM Pro.

They can operate in several modes and gain settings, which essentially change their gain, readout noise (RON) and fullwell capacity (FWC). In this work, we have

[1]https://www.qhyccd.com/scientific-camera-qhy600pro-imx455/

[2]https://www.qhyccd.com/scientific-camera-qhy411-qhy461/

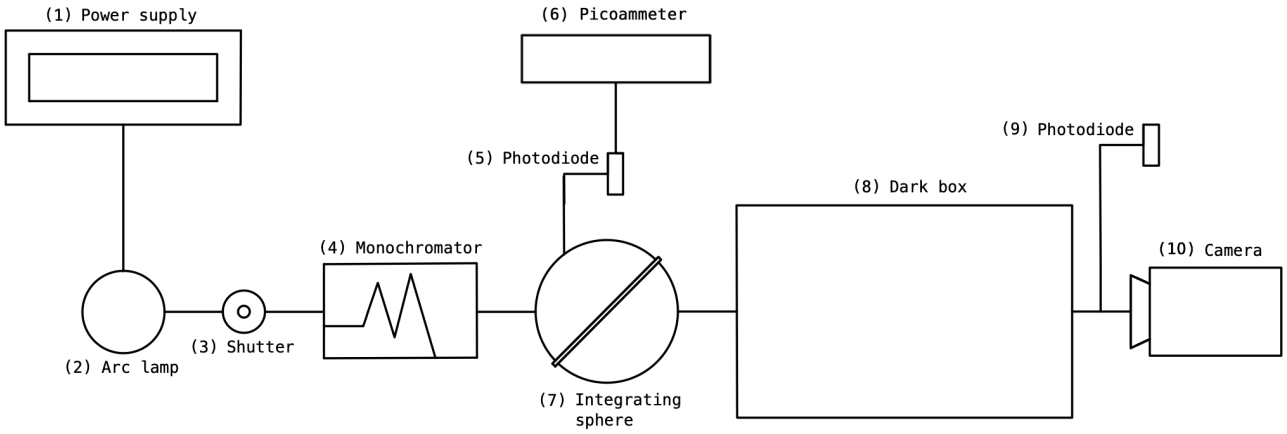

Figure 1. Diagram of the optical test bench setup, with the (1) Newport 68945 digital power supply, (2) Newport 66902 75 W Xe arc lamp, (3) Newport 76994 shutter, (4) Newport Oriel Cornerstone monochromator, (5) Hamamatsu S1336-5B1 photodiode, (6) Labsphere SC6000, (7) Labsphere US-080-SF/SL integrating sphere, (9) Hamamatsu S2281 photodiode and (10) QHY600M Pro / QHY411M.

focused on those considered most appropriate for use in Astronomy, as they keep a good balance between these characteristics. These are Mode #1 (High Gain Mode) and gain setting 0 on the QHY600M Pro and Mode #4 and gain setting 0 on the QHY411M, although some results for other modes are also shown.

The evaluation of the sensors was performed using existing experimental equipment, available at the Astronomical Image and Sensors Laboratory (Laboratorio de Imagen y Sensores para Astronomía, LISA), at the Instituto de Astrofísica de Canarias (Tenerife, Spain). The setup is schematically shown in Figure 1.

The sky tests were performed with two of the robotic telescopes (Telescopios Abiertos Robóticos, TAR) of the Teide Observatory (Tenerife, Canary Islands, Spain). The QHY600M Pro was installed on the prime focus of TAR03, 0.46-m f/2.8 C18 reflector telescope, on a Planewave L500 AltAz mount. A ROI of 4096×4096 was used, giving a FOV of 41.1×41.1 arcmin with 0.6 ”/px. The QHY411M was mounted on a 80-cm f/6.85 AltAz telescope of the TTT (Two-meter Twin Telescope) project. A FOV of 4096×4096 was used and the plate scale was 0.14 ”/px.

3. RESULTS

3.1. Readout noise and Salt & Pepper effect

Due to the fact that each pixel has its own capacitor+amplifier, the noise introduced in the readout process may be different for each pixel. 21 frames have been stacked by taking the standard deviation across each pixel, to obtain the readout noise (RON) particular to each of them. The distribution of these RON for both cameras is shown in Figure 2. In the case of the single-channel CCDs, these values follow a Gaussian distribution–whose model has been included with a dotted line–as all pixels are measured by a single output node. For sCMOS sensors, the distribution at low standar deviation is similar to its CCD equivalent, but, beyond the peak, the curve flattens out into a long tail rather than dropping steeply as in the gaussian model. This suggests the presence of pixels with higher RONs than average, which are observed to be homogeneously distributed across the sensor. It can be seen that, in the selected modes of operation for each camera, their distributions are shifted until shortly after the peak, where they start to converge for high RON values, from 6 e^- onwards. The median is around 2.8 e^- for the QHY600M Pro and 3.25 e^- for the QHY411M. The rms is indicated in the plots with a vertical line, being 3.5 e^- for the QHY600M Pro and 3.8 e^- for the QHY411M. Readout noise higher than this values is only found for 22% and 17% of the pixels respectively.

For a more detailed insight into the behaviour of these pixels with high standard deviation, 1000 consecutive bias frames were obtained with the QHY600M Pro. In a small central region of 20×20 pixels the temporal average and standard deviation of all frames has been taken, which is shown in the upper part of Figure 3. Most of the pixels have an average signal around 171 ADU and a dispersion below the RON, as expected. However, there are some of them that show anomalous patterns in the average value, the standard deviation or both at the same time. Several pixels have been selected as samples, showing the time evolution of the signal in the lower plots. As a reference, a pixel with normal values of average signal and deviation has been taken, following a normal distribution over the 1000 frames, with mean 170.4 ADU and standard deviation 3.69 ADU. The pixel labeled as S&P 1 also has an average signal similar to the others, with a slightly higher standard deviation of 6.42 ADU but still close to the RON obtained in the previous section. How-

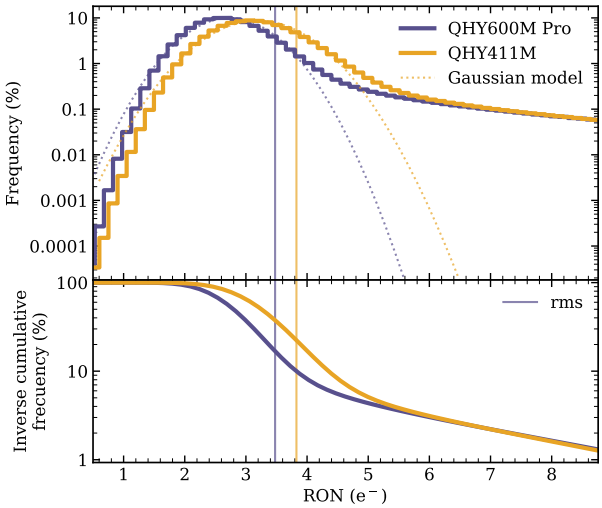

Figure 2. Readout noise distribution, obtained as the standard deviation across each pixel of 21 consecutive bias frames, for the QHY600M Pro (blue) and the QHY411M (yellow). The gaussian model of the CCD equivalent is included as dotted curves. The lower plot shows the cumulative inverse frequency, which indicates the percentage of pixels that have a RON higher than the value on the x axis. The root mean square of each distribution is indicated by a vertical line.

ever, the temporal distribution reveals how some points, 5.5% of the total, appear both above and below the average signal, with a gap of about 20 ADU, more than 3 times the RON–red dots in the plots below. Other pixels show the same effect more often, e.g. S&P 3, where 19.3% of the 1000 frames show an anomalous value of ±60 ADU. This is revealed by a high standard deviation of 23.6 ADU which, although it can be understood as a high RON in its electronics, it should be noted that its distribution is not a wide gaussian, but a set of 3 normal distributions, the main centred on 171 ADU and two smaller ones corresponding to these random leaps to higher and lower values at 110 and 230 ADU. The S&P 2 pixel shows jumps at the same levels, but with a higher proportion of values in the upper one, 10.6% of the total, than in the lower one, 3%, so that the signal obtained in the average frame, 174.5 ADU, is deviated from the other pixels, as it is shown in the image.

These jumps between above-average and below-average signal values are observed when blinking between images, regardless of their exposure time and temperature. A pattern of bright and dark pixels that appear and disappear from one frame to the next one is observed. This effect, sometimes referred as *Salt & Pepper*, is Random Telegraph Noise (RTN). RTN is the fluctuation of the signal between discrete levels as a consequence of the capture and emission of charges by defects or traps located very close to the Si-SiO_2 interface [10]. In scaled CMOS detectors, this trapping process causes a shift in the relation between the drain current of the MOS transistor and the gate voltage, discretely increasing or decreasing

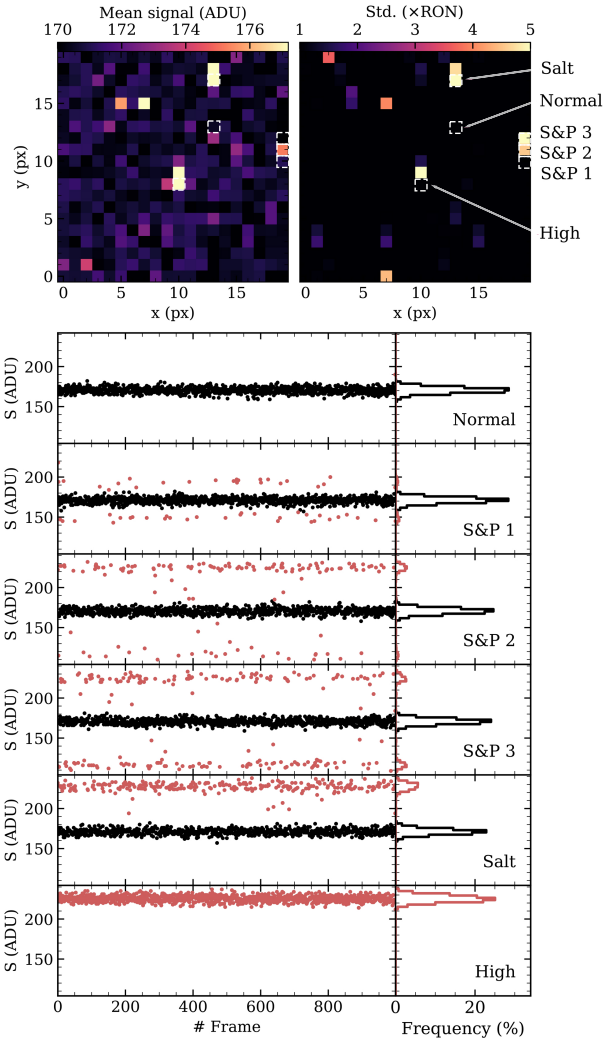

Figure 3. Top: temporal mean signal (left) and standard deviation n terms of readout noise (right) obtained in a 20×20 pixel central region of 1000 bias frames taken consecutively with the QHY600M Pro. Bottom: signal vs frame number for some relevant pixels identified in the images above. Points within the average value of the master bias ±3×RON are shown in black, with outliers identified in red. On the right, the signal distribution of these pixels is displayed.

the offset level, which fluctuates as random trapping and de-trapping of charges, either electrons or holes, happens [7].

3.2. Dark current

To characterise the dark current (DC), 5 dark frames of 1000 s of exposure time were taken, a master bias taken just before was subtracted and they were median stacked. This was done for various temperatures: from 5C to -10C on the QHY600M Pro and from -5C to -20C on the QHY411M, on which water cooling was installed for these tests. The DC distribution in electrons per pixel and second of exposure is shown in Figure 4. The distribution curves have similar shapes, with a shift towards higher DC with increasing temperature. When the peak is reached, DC drops rapidly towards a smooth hump, from which it drops back down again. This hump corresponds to a set of pixels with exceptionally higher DC, which are seen in the images as pixels with a higher signal that is steady from frame to frame and increases linearly with exposure time. At -10C, only 0.024% of the QHY600M Pro pixels and 0.005% of the QHY411M have a DC greater than RON. These warm pixels, moreover, have signals lower than the saturation level, so they can be corrected with an appropriate master dark.

3.3. Quantum efficiency

Central wavelengths in the range between 350 and 1100 nm with 25 nm steps were selected in the monochromator. The grating configuration was set to have an outcoming light with 1 nm bandwidth. The QHY600M Pro was placed at 13.3 mm from the exit of the dark box, which is 30 mm apart from the Hamamatsu S2281 photodiode. The total distance between the IMX455 sensor and the photodiode, considering the back focus distance of the camera, was 66.8 mm. In the case of the QHY411M, it could be placed in contact with the box, so the total distance between the photodiode and the IMX411 sensor was 58.5 mm. Both cameras were binned 4×4 to have enough signal with exposure times shorter than 10 seconds at those wavelengths where they are less efficient.

Three images were taken at each wavelength step, a masterbias created at the beginning of the series was subtracted to all of them and they were stacked with the 3-sigma-clipped median. Simultaneously, the output intensity of the photodiode placed at the secondary port of the integrating sphere was measured with the picoammeter for approximately 30 seconds, taking an average value. The observed fluctuations in this value were always less than 2%. The systematic uncertainty of the method is estimated to be around 3%. To avoid vignetting effects at the edges of the dark box-camera junction, a central ROI of 1000×1000 binned pixels was used to obtain the median signal S, after checking that there were no inhomogeneities in the sensor illumination in that area. The exposure time t_{exp} had to be varied throughout wavelength

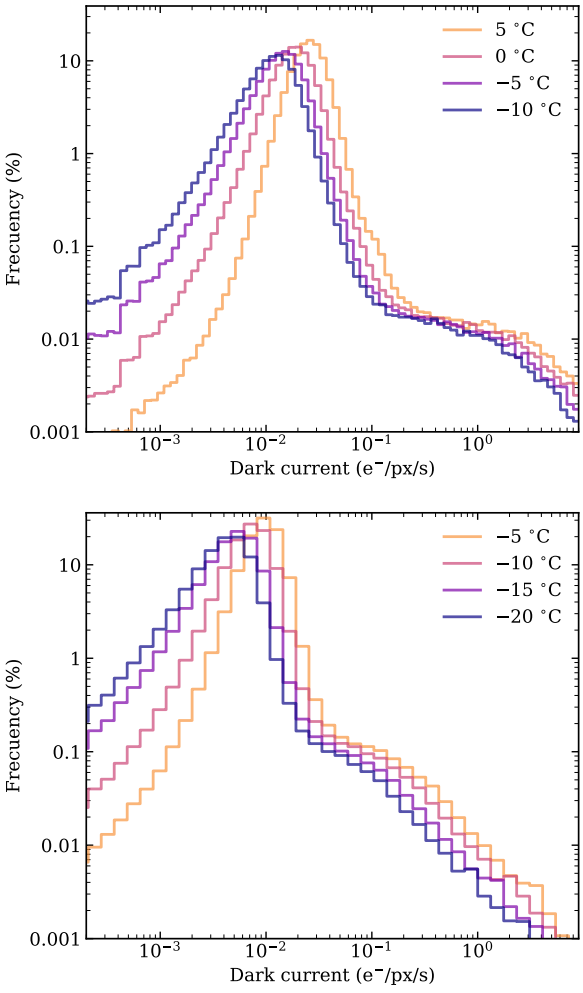

Figure 4. Dark current distributions for the QHY600M Pro (top) and the QHY411M (bottom). They have been obtained as the median stacked set of 5 dark frames with an exposure time of 1000 seconds.

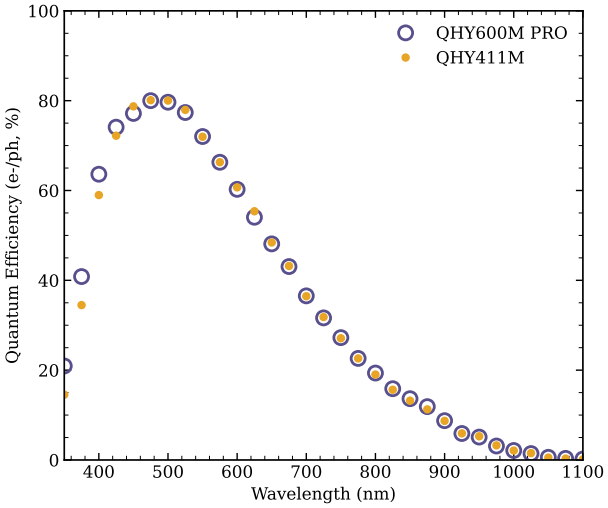

Figure 5. Absolute quantum efficiency curves of the QHY600M Pro (blue open circles) and the QHY411M (yellow dots).

steps to keep all measurements in the shot noise dominated region, between 1000 and 40000 ADUs.

The QE curves for the sensors are shown in Figure 5. Both show very similar behaviour, with a peak efficiency of 80% at 475 nm, a steep drop at shorter wavelengths and a gradual decrease towards the redder ones, with a QE of 40% at 700 nm and 10% at 900 nm. back-illuminated sCMOS sensors with reduced pixel size such as the IMX455 and IMX411 have a typical silicon substrate thickness of around 3 microns [9]. This optimises the photon absorption in the visible range, but makes the less energetic photons, which have a higher penetration capability, more unlikely to be detected. Improving efficiency in the red and near-infrared requires, without any additional red enhancement technology, a thicker substrate which, with such small pixels, would lead to image degradation due to crosstalk between adjacent pixels. This is the reason for the poor performance at longer wavelengths.

4. ON-SKY TESTS

Both cameras have been extensively tested on images taken with telescopes, obtaining photometric accuracies as expected for the characteristics described above. In the case of the QHY600M, it was installed at the prime focus of a 0.46-m f/2.2 telescope. Figure 6 shows the phased light curve of asteroid (3200) Phaethon, observed for 6 consecutive hours. At the time of observation, the object had an apparent magnitude of V=17 and was moving at a speed of 1.6”/min. The photometric uncertainties obtained are in the order of hundredths of a magnitude and the rotation of the asteroid, with an amplitude of 0.13 mag, is clearly detectable. This camera is a very suitable choice for very fast telescopes with primary focus, as its small size and cylindrical shape drastically reduce obscuration. With a pixel size of 3.76 microns, it also allows

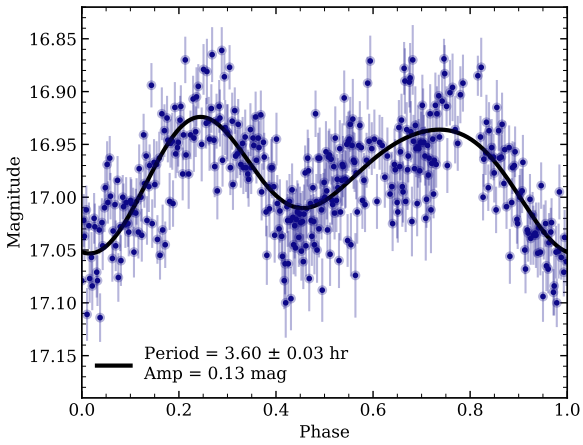

Figure 6. Phased light curve of the asteroid (3200) Phethon, obtained with the QHY600M mounted at the prime focus of a 0.46-m f/2.2 telescope, clear filter.

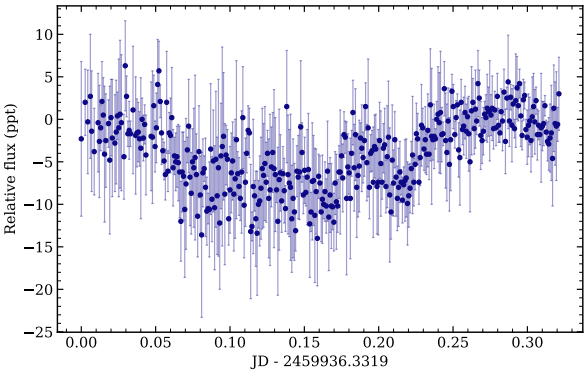

Figure 7. Transit of the exoplanet TOI-1135 observed with QHY411M mounted on a Nasmyth focus of the TTT-2 telescope at 0.80-m and f/6.85, SDSS g’ filter.

to obtain a plate scale very suitable for excellent seeing sites such as the Teide Observatory. Furthermore, given its low readout noise and no readout time, it is possible to take more short frames, so that the asteroid does not come out with a trace and combine them by aligning with the object or the stars, allowing fainter objects to be reached with very little time lost. This also allows to study very fast rotating objects with a good temporal sampling [11].

Figure 7 shows a transit of the exoplanet TOI-1135, observed with the QHY411M mounted on one of the Nasmyth foci of the TTT-2 telescope, 0.80-m f/6.85, SDSS g' filter, with a plate scale of 0.14"/px. In this case the PSF was oversampled, with stars of about 8 px FWHM, which allowed us to observe very bright objects–the star was magnitude V=9.6–with longer exposure times without reaching the saturation point. This is especially useful in this case where, if an equivalent CCD were used, it would require some defocusing. In addition, by taking short exposures, the time lost on a CCD could be equivalent to or even longer than the exposure time, making it very inefficient. With the QHY411M, the exposure time could be extended, improving photometric accuracy, and the readout time is almost non-existent. Having such small plate scales, while generally undesirable, also allows these cameras to be used in other scientific applications such as astrometry of fast moving objects or lucky imaging.

5. CONCLUSION

In the previous sections, the key features of the QHY600M Pro and QHY411M cameras as scientific instruments have been discussed in detail. They have characteristics that make them very suitable for general use, although some issues like the Salt & Pepper effect need to be addressed. The two instruments present characteristics compatible with their use in Astronomy. Their low cost, power consumption and replicability make both cameras a very suitable solution, highlighting especially their high frame range, near-zero readout time and low readout noise. Regarding the quantum efficiency, although the curve obtained here is slightly lower than that reported by the manufacturer, 80% at 500 nm is an acceptable performance for many scientific programs and in general similar or better than other CCD sensors in the same cost range. An improvement in efficiency towards redder wavelengths should be achieved in the next few years so that sCMOS sensors can be used on a wider variety of observational targets.

The small pixel size makes these sensors generally not suitable for slow focal length systems, except for dedicated programs such as high spatial resolution or lucky imaging, for instance. Nevertheless, they can be very valuable in fast telescopes with larger fields and higher plate scales, allowing better sampling of the PSF, being their manageability and small size and weight also a very interesting, for example, prime focus telescopes. The combination of such telescopes and cameras permit to obtain very large field of view images with plate scales with reasonably good sampling of the PSF. For instance, a 11" f/D=2.2 telescope like the Celestron RASA11 with a QHY600 camera produce images of 7.5 deg^2 field of view and a plate scale of 1.27 "/pix that are excellent options for surveys like ATLAS (Licandro et al., *New telescopes and radars* session).

ACKNOWLEDGMENTS

The authors declare no conflict of interest or relationship with the manufacturers of the cameras tested. This research has been partially funded by Light Bridges, SL. which provided the QHY411M and Andor iKon-L 936 cameras for the tests presented here.

REFERENCES

1. Astropy Collaboration et al., 2013, A&A, 558, A33.
2. Bigas M., Cabruja E., Forest J., Salvi J., 2006, Microelectronics J., 37, 433.
3. Coates C., Fowler B., Holts G., 2009, White Paper: Scientific CMOS technology, a high-performance imaging breakthrough.
4. Fossum E. R., 1997, Nucl. Instrum. Methods Phys. Res. A, 395, 291.
5. Law N. M., et al., 2022, PASP, 134, 035003
6. Karpov S., Bajat A., Christov A., Prouza M., Beskin G., 2021, arXiv e-prints, p. arXiv:2101.01517
7. Martin-Martinez J., Rodriguez R., Nafria M., 2020, Advanced characterization and analysis of random telegraph noise in CMOS devices.
8. Princeton Instruments 2016, New Scientific CMOS Cameras with Back–Illuminated Technology. Technical Note.
9. Yokogawa S., et al., 2017, Scientific Reports, 7, 3832.
10. Uren M., Day D., Kirton M., 1985, Applied physics letters, 47, 1195.
11. Licandro et al. 2023, submitted to MNRAS.